ingegneria sismica
International Journal of Earthquake Engineering
Anno XLIII - Num. 2 - 2026

Study on Dynamic Slope Detection and Automatic Tracking and Positioning Accuracy Improvement Based on Kalman Filter Algorithm

Hui Feng[1,*], *Tiewen Lu*[1], *Weiwei Jiang*[1] *and Hang Gu*[1]

[1] School of Intelligent Engineering Technology, Jiangsu Vocational College of Finance and Economics, Huai'an, 223003, China

SUMMARY: *In this paper, we first construct a vehicle kinematics model using longitudinal acceleration and implement real-time ramp angle estimation by Kalman filter algorithm. Subsequently, it is improved to a dynamics estimation method with extended Kalman filter, and the results of the two estimation nodes are data fused by analyzing the shortcomings of the dynamics and vision schemes in order to achieve redundant and complementary results. The average absolute error and root-mean-square error of this paper's model, VB-EKF, are reduced by at least 50% compared with the comparison model, which reduces the oscillation error of the estimation results when the vehicle enters and exits the ramp; and the estimation accuracy of the VB-EKF model in special working conditions is significantly improved. The real-vehicle test of roadway lateral slope estimation based on VB-EKF shows that the average absolute error and root-mean-square error of the method are reduced by more than 60% compared with the comparison model, and its estimation error is controlled within 2%, with better robustness and stability of the model. This paper provides a new and more accurate method for dynamic slope detection and automatic tracking and positioning accuracy estimation.*

KEYWORDS: *Kalman filter algorithm; slope estimation; machine vision; data fusion*

1 Introduction

Slope is an important concept in geography and civil engineering, which is directly related to the design and construction of roads, buildings and terrain. Accurately detecting and analyzing slope can assist in rational planning of geography, designing reasonable slopes, reducing the risk of road traffic accidents, improving driving comfort, reducing energy consumption, and enhancing building stability and improving building safety [1-4]. For example, a slope greater than 10% is likely to lead to insufficient vehicle power, affecting transport efficiency, and when the slope increases, tire wear increases and costs increase [5]. In terms of terrain design, by detecting slopes in geographic terrain, the complexity and diversity of the terrain can be assessed, which helps to produce accurate terrain models and provide basic data for geological studies [6]. In addition, in agricultural planning and urban storm drain design, reasonable slopes can increase the seedling rate of agricultural machine seeding, reduce the risk of soil erosion, drain water quickly and effectively, reduce the risk of urban flooding, and protect water sources and soil [7-9].

In the current road slope detection work, the inspectors generally use static detection method, that is, the use of slope ruler on each section of the road point by point detection, each section of the test several times, in order to obtain accurate slope information, this detection method is

*jscjfenghui@163.com
https://doi.org/10.65102/is20261004
Published: 30 April, 2026

not only a huge amount of workload, but also consumes a long time, and the accuracy of the resulting data is also relatively low. Gradually, some researchers have proposed other methods. Literature [10] utilizes an adjustable camera to capture pavement slope data, and upgrades this captured two-dimensional image into three-dimensional point cloud data, which is processed by real-time data correction to increase the accuracy of the data, in order to detect the slope. Literature [11] describes three methods of slope value estimation, which are geometric principles, covariance, and local features, by analyzing and calculating the images captured instantly by the camera, the first two methods emphasize on the use of two-dimensional road lines, and the method of local features is based on the use of the camera images to estimate the actual slope changes. Literature [12] combines machine vision and spatial convolutional neural network algorithms to capture and compute the lane line information in front of the vehicle to compute the road side slope values respectively. Literature [13] utilized open LiDAR point cloud analysis to automate the detection of rock avalanche road gradients with up to 100% accuracy while maintaining high detection speed. However, most of the studied dynamic detection methods are unstable in terms of correctness and consider a single factor.

In addition, the accuracy of the positioning correction after road slope detection is affected by both geographical environmental factors such as trees and movement carriers, and the satellite signal is weak, the positioning error increases, which is not conducive to the implementation of automatic tracking and positioning [14, 15]. If the dynamic detection method can be used, through some corresponding equipment or tools, to obtain the slope condition of each point of the whole journey, it will improve the efficiency of slope detection and automatic tracking and positioning accuracy. The Kalman filter (KF) algorithm, on the other hand, is a technique used for estimating the system state, which dynamically adjusts the estimate of the system state by fusing the sensor measurements and the predictions of the system model to provide an optimal estimate of the system state [16]. It has a wide range of applications and plays an important role especially in the fields of navigation, image processing, and robotics. As mentioned in the literature [17], the KF algorithm can cope with the positioning errors caused by the short path effect defects of GNSS, but the positioning accuracy still needs to be improved, so the authors added a climbing motion model to constrain the short-range multipath effect in the adaptive KF algorithm, which greatly improves the accuracy of positioning. Literature [18] utilizes the extended KF algorithm to calculate the road slope and combines the forgetting factor recursive least squares method to calculate the vehicle mass, which realizes the dynamic estimation of the two. Literature [19] constructed a road slope estimation model by the improved Sage-Husa adaptive KF, and the vehicle's form speed and road slope roughness are used as the input values of the model, which can instantly output the current slope value.

In this paper, we first preprocess the vehicle speed and longitudinal acceleration signals input from the bus, and construct the Kalman filter equation to estimate the road slope based on the relationship between slope and vehicle speed and longitudinal acceleration. Then, considering the influence of the noise variance parameter on the slope estimation results in the Kalman filtering process, the Extended Kalman Filtering Dynamics road slope estimation model filter is designed to optimize the slope estimation results. In order to get the estimation results closer to the real values, the dynamics model will be further investigated in this paper to derive the extended Kalman filter dynamics lateral slope estimation model. Subsequently, its estimation results are fused with the visual estimation results by Kalman filtering, and the real-time and effectiveness of the slope estimation algorithm is verified by simulation test and real vehicle test.

2 Dynamic slope detection and localization algorithm based on VB-EKF algorithm

2.1 Ramp angle estimation based on Kalman filter algorithm modeling

2.1.1 Vehicle kinematic modeling

The vehicle longitudinal acceleration [20] signal acquired by the sensor consists of the component of gravity acceleration in the ramp direction and the longitudinal component of the self-vehicle acceleration.

According to the principle of longitudinal acceleration acquisition, it is known:

$$a_{senx} = gsini + a_{CANv} \tag{1}$$

where a_{senx} is the longitudinal acceleration collected by the acceleration sensor, g is the gravitational acceleration, i is the road ramp angle, $a_{CANv} = dv/dt$ is the acceleration estimation of the vehicle, v is the bus speed signal, and t is the time. When a_{senx} and a_{CANv} are known, the ramp angle estimation can be calculated according to equation (1). However, the accuracy of the speed signal of the bus is low, and the a_{CANv} component fluctuates greatly when the sampling period is short. The actual ramp angle takes the vehicle pitch angle signal collected by the sensor as a reference. Due to the drastic jitter of the roadway ramp angle estimation, the estimation result has a large error and the data cannot be used.

2.1.2 Kalman filter ramp angle estimation algorithm

(1) Kalman filtering

The Kalman filter algorithm [21, 22] is relatively mature, and its iterative process includes time update and measurement update. The time update is to predict the state and error covariance at the next moment: the measurement update mainly calculates the Kalman gain coefficient, and the state value and error covariance at the current moment are calculated according to the Kalman gain coefficient. The filtering equations are as follows:

$$\begin{cases} \hat{x}_{\bar{k}} = A\hat{x}_{k-1} + Bu_{k-1} \\ P_{\bar{k}} = AP_{k-1}A^T + Q \\ K_k = \dfrac{P_{\bar{k}}H^T}{HP_{\bar{k}}H^T + R} \\ \hat{x}_k = \hat{x}_{\bar{k}} + K_k(z_k - H\hat{x}_{\bar{k}}) \\ P_k = (I - K_kH)P_{\bar{k}} \end{cases} \tag{2}$$

where: $\hat{x}_{\bar{k}}, \hat{x}_k$ is the k-moment system state prediction, output value, $P_{\bar{k}}, P_k$ is the k-moment system state covariance prediction, output value, respectively, K_k is the Kalman gain at k moments, I is the unit matrix, and Q, R are the process noise variance and observation noise variance, respectively.

(2) Longitudinal kinematic equation discretization

Define the system state quantity $x=[v\ a_{senx}i]^T$, the observation quantity $z=[v\ a_{senx}]^T$, and discretize the state system, taking $\sin i=i$ when the ramp angle is small:

$$\begin{cases} v(k)=v(k-1)+[a_{senx}(k-1)-gi(k-1)]T+w_1(k-1) \\ a_{senx}(k)=a_{senx}(k-1)+w_2(k-1) \\ i(k)=i(k-1)+w_3(k-1) \end{cases} \tag{3}$$

where: $v(k)$ is the vehicle speed at the current moment; $a_{senx}(k)$ is the acceleration sensor measurement result at the current moment; $i(k)$ is the ramp angle at the k moment; T is the discretization time period, and according to the actual bus signals, the sampling period is set to 10ms; $w_1(k), w_2(k), w_3(k)$ are the process noise for velocity, acceleration and ramp angle, respectively.

Therefore, the discretized equation of state expression is given by:

$$\begin{cases} x(k)=\tilde{A}x(k-1)+w(k) \\ z(k)=\tilde{H}x(k)+v(k) \end{cases} \tag{4}$$

where: $A=\begin{bmatrix} 1 & T & -gT \\ 0 & 1 & 0 \\ 0 & 0 & 1 \end{bmatrix}$, $\tilde{H}=\begin{bmatrix} 1 & 0 & 0 \\ 0 & 1 & 0 \end{bmatrix}$, $w(k)=[w_1(k), w_2(k), w_3(k)]^T$, $v(k)=[v_1(k), v_2(k)]^T$, $v_1(k), v_2(k)$ are the observation noise for velocity and acceleration, respectively.

2.2 Filter fusion model for slope estimation

In order to get the estimation results closer to the real values, the dynamics model will be further investigated in this section to derive the extended Kalman filter dynamics lateral slope estimation model, and subsequently its estimation results will be fused with the visual estimation results by Kalman filtering. The filter fusion process for Kalman filter-based slope estimation is shown in Fig. 1.

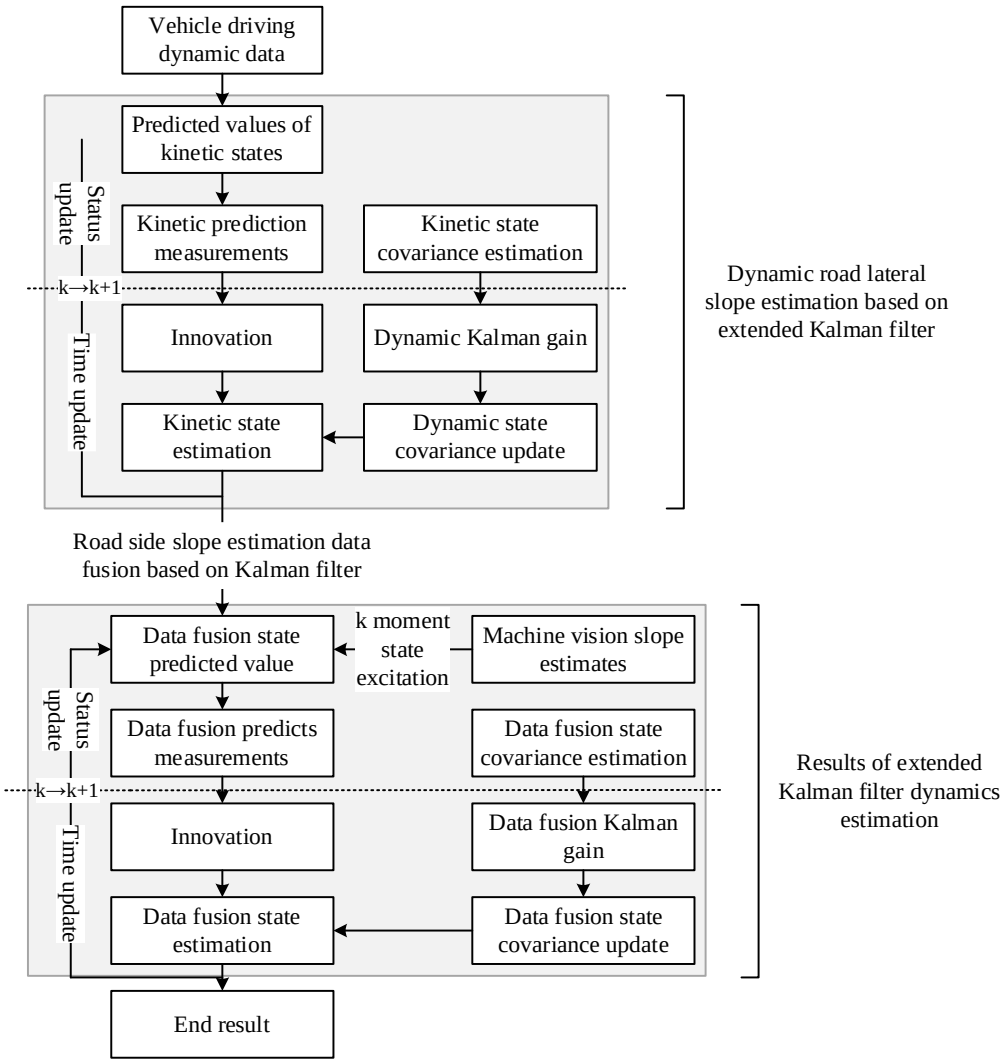

Figure 1: Based on kalman filtering slope estimation filter fusion process

2.2.1 Extended Kalman filter dynamics road slope estimation model

The Kalman filtering algorithm is considered to reduce the fluctuation as well as the error of the dynamics estimation results. The classical Kalman filter model equations are linear equations, which cannot be directly applied to nonlinear systems, so this section applies the extended Kalman filter algorithm [23] to the dynamics slope estimation model to obtain more accurate and less fluctuating dynamics estimation results, in order to provide reliable data for the subsequent fusion algorithm.

According to the vehicle degree of freedom model can be obtained:

$$\begin{cases} m(\dot{v}+ur) = F_{yrw} + F_{yfw} - mg\sin\phi \\ I_z\dot{r} = aF_{yrw} - bF_{yfw} \\ F_{yrw} = K_f\left(\delta - \dfrac{v+ar}{u}\right) \\ F_{yfw} = K_r\left(\dfrac{-v+br}{u}\right) \end{cases} \tag{5}$$

where m is the mass of the vehicle; v is the lateral speed of the vehicle; F_{yrw} is the lateral force at the rear wheels of the vehicle; F_{yfw} is the lateral force at the front wheels of the vehicle; u is the longitudinal speed of the vehicle; r is the vehicle's transverse angular velocity; ϕ is the angular estimate of the roadway's lateral gradient, $\phi = \phi_v + \phi_t$; a is the distance from the center of mass of the vehicle to the front axle; b is the distance from the center of mass of the vehicle to the rear axle; and I is the rotational inertia of the vehicle body around the Z axis.

A nonlinear model can be obtained by further analyzing the above equation. Assuming that the longitudinal velocity of the vehicle is slowly changing during its travel, at each step, the time-varying nonlinear system can be approximated by a linear process:

$$\begin{cases} \dot{x}_d = A_d(t)x_d + B_d(t)u_d \\ y_d = C_d(t)x_d + D_d(t)u_d \end{cases} \tag{6}$$

where $x_d = [v_y, r]^T$ is the state vector, $y_d = [a_y, r]^T$ is the measurement output vector, $u_d = \delta$ is the control input vector, and the matrices $A_d(t), B_d(t), C_d(t)$ and $D_d(t)$ are shown in the following equation:

$$\begin{cases} A_d(t) = \begin{bmatrix} \dfrac{-K_f - K_r}{mu(t)} & -u(t) - \dfrac{aK_f - bK_r}{mu(t)} \\ \dfrac{-aK_f + bK_r}{I_z u(t)} & \dfrac{-a^2K_f - b^2K_r}{I_z u(t)} \end{bmatrix} \\ B_d(t) = \begin{bmatrix} \dfrac{K_f}{m} & \dfrac{aK_f}{I_z} \end{bmatrix}^2 \\ C_d(t) = \begin{bmatrix} \dfrac{-K_f - K_r}{mu(t)} & -\dfrac{aK_f - bK_r}{mu(t)} \\ 0 & 1 \end{bmatrix} \\ D_d(t) = \begin{bmatrix} \dfrac{K_f}{m} & 0 \end{bmatrix}^T \end{cases} \tag{7}$$

Can be derived from equation (5):

$$\dot{v} = \frac{-(K_f + K_r)}{mu}v - \left(u + \frac{aK_f - bK}{mu}\right)r + \frac{K_f}{m}\delta - g\sin\phi \tag{8}$$

Since the measured values of the sensors are partially perturbed, there:

$$\begin{aligned} a_y^{sen} &= a_y + g\sin\phi + d = \dot{v} + ur + g\sin\phi + d \\ &= \frac{-(K_f + K_r)}{mu}v - \frac{aK_f - bK_r}{mu}r + d + \frac{K_f}{m}\delta \end{aligned} \tag{9}$$

where d is the sensor bias. At this point, the extended Kalman filter can be constructed based

on the above equation, which will be forward Eulerian to further obtain the discrete model:

$$\begin{cases} \hat{x}_d[k+1] = (A_d[k]\Delta t + I_4)\hat{x}_d[k] + B_d[k]\Delta tou_d[k] + w_d[k] \\ \hat{y}_d[k] = C_d[k]\hat{x}_d[k] + D_d[k]u_d[k] + v_d[k] \end{cases} \tag{10}$$

At this point in the equation, $x_d = [v_y, r, \sin\phi, d]^T : y_d = [a_y^{sen}, r]^T$ where Δt is the sampling period.

$w_d(k)$ and $v_d(k)$ are the process noise and measurement noise Eqs. $A_d(t), B_d(t), C_d(t)$ and $D_d(t)$ turn out:

$$\begin{cases} A_d(t) = \begin{bmatrix} \dfrac{-K_f - K_r}{mu(t)} & -u(t) - \dfrac{aK_f - bK_r}{mu(t)} & -g & 0 \\ \dfrac{-aK_f + bK_r}{I_z u(t)} & \dfrac{-a^2K_f - b^2K_r}{I_z u(t)} & 0 & 0 \\ 0 & 0 & 0 & 0 \\ 0 & 0 & 0 & 0 \end{bmatrix} \\ B_d(t) = \begin{bmatrix} K_f & aK_f & 0 & 0 \\ m & I_z & 0 & 0 \end{bmatrix} \\ C_d(t) = \begin{bmatrix} -K_f - K_f & -\dfrac{aK_f - bK_f}{mu(t)} & 0 & 1 \\ 0 & 1 & 0 & 0 \end{bmatrix} \\ D_d(t) = \begin{bmatrix} K_f & 0 \\ m & 0 \end{bmatrix}^T \end{cases} \tag{11}$$

In order to obtain the Jacobi matrix, the linearization of Eq. (10) for the partial derivatives leads to the correlation matrix of the extended Kalman filter as:

$$\Phi = \frac{\partial f}{\partial x_d}, H = \frac{\partial h}{\partial x_d} \tag{12}$$

Then the time update equation for the state space of the system is obtained from the above equation:

$$\begin{cases} \hat{x}_d(k) = \Phi(k)\hat{x}_d(k-1) + E(k)u_d(k-1) \\ \hat{y}_d(k) = H(k)\hat{x}_d(k) \\ P(k) = \Phi(k)H(k)\Phi(k) + Q(k) \end{cases} \tag{13}$$

Temporal updating is the process of predicting the state vector and the output vector of the next moment from the state vector of the current moment, and calculating the error covariance after updating. The difference between the predicted value and the actual output value at the next moment is taken as the new interest, which is used to calculate the Kalman gain value, and the state prediction value is corrected according to the new interest and the Kalman gain value

to obtain the a posteriori estimation value, and the state covariance is further updated. The new interest defined by Kalman filtering is as follows:

$$e(k) = y_d(k) - \hat{y}_d(k) \tag{14}$$

The new interest is very important for the Kalman filter system, which provides key information for the feedback correction of the system and directly affects the final estimate. Under the premise of calculating the new interest, the estimates can be further updated and predicted:

$$\begin{cases} K(k) = \dfrac{P(k)}{H(k)P(k)H(k)^T + R(k)} \\ \hat{x}_d(k) = \hat{x}_d(k) + K(k)e(k) \\ \hat{P}(k) = (I - K(k)H(k)P(k)) \end{cases} \tag{15}$$

2.2.2 Extended Kalman Filter and Machine Vision Fusion Methods

The Extended Kalman Filter fused with machine vision for lateral slope estimation (referred to as VB-EKF) is as follows: by first considering the dynamics estimation results and the vision estimation [24] results as sensor measurements, a linear dynamic system can be built:

$$\begin{cases} x_k = Ax_{k-1} + Bu_{k-1} \cdot \Delta t + q_{k-1} \\ y_k = Hx_k + r_k \end{cases} \tag{16}$$

where x_{k-1} is the slope estimation result of the dynamics at the $k-1$ moment; u_{k-1} is the slope estimation result of the machine vision at the $k-1$ moment: q_k is the process noise; r_k is the observation noise; Δt is the step size; y_k is the observed value at moment k. Since the road gradient generally does not undergo large abrupt changes, A, H and B can be regarded as the unit matrix.

At this point, assuming that the covariance matrices of process noise and observation noise are Q and R respectively, the a priori estimated covariance at k moments is $P(k|k-1)(k|k-1)$ and the a posteriori estimated covariance is $P(k|k)$, then one iteration of Kalman filtering process is:

State Prediction:

$$x_k(k|k-1) = x_k(k-1|k-1) + u_{k-1} \cdot \Delta t \tag{17}$$

Kalman gain matrix:

$$K(k) = P(k|k-1)[P(k|k-1) + R]^{-1} \tag{18}$$

Computing Kalman filtering new interest:

$$e(k) = y(k|k) - y(k|k-1) \tag{19}$$

Status Follow-Up:

$$x(k \mid k) = x(k \mid k-1) + K(k)e(k) \tag{20}$$

Calculate the estimated covariance matrix:

$$P(k \mid k) = (I - K(k))P(k \mid k-1) \tag{21}$$

3 Analysis of the application effect of VB-EKF algorithm in slope detection and positioning accuracy

3.1 Simulation experiment of road slope estimation based on VB-EKF

In order to investigate the effectiveness of the lateral slope estimation method based on the fusion of extended Kalman filter and machine vision, a human-vehicle-road model is built in the CarSim-Simulink-PreScan environment for simulation verification. Set the lateral slope and dynamic parameters of the road, install virtual sensors on the vehicle body, and introduce Gaussian white noise to simulate the real environmental noise to interfere with the sensor measurements, build the same ramp through PreScan, and install a camera above the setup vehicle at a distance of 1.2m from the ground to obtain the road image in front of it, and synchronize the video frame rate with the frequency of sensor data acquisition, and use Simulink to Build a slope estimation model to estimate the slope.

The slope of the road in the road model is the slope data of a randomly selected section with a total mileage of 15030m. The maximum value of the random slope is 14.25% and the minimum value is -3.07%.

In order to evaluate the estimation effect of the VB-EKF road slope estimation method proposed in this paper, the EKF and EKFK slope estimation methods are used as a control, and 10 slope estimation simulations are performed for each of the three methods. In order to objectively evaluate the estimation effect of the three methods, the estimation effect of the three methods is evaluated by taking the mean absolute error MAE and the root mean square error RMSE as the indexes, and the specific formula for the evaluation indexes is:

$$\begin{cases} MAE = \dfrac{1}{n}\sum_{i=1}^{n} \mid e_i - a_i \mid \\ RMSE = \sqrt{\dfrac{1}{n}\sum_{i=1}^{n}(e_i - a_i)^2} \end{cases} \tag{22}$$

where: n is the length of the slope sequence; e_i is the estimated value of the slope at moment i; a_i is the actual value of the slope at moment i.

3.1.1 Objective evaluation of simulation slope estimation results

Figure 2 shows the objective evaluation index values of the simulation slope estimation results. The results show that the MAE value of the model VB-EKF in this paper is reduced by 92.13% and 55.63% than the EKF algorithm and the EKFK algorithm, respectively; the RMSE value is reduced by 92.85% and 67.52%. On the whole, the VB-EKF estimation accuracy is greatly improved over the other two algorithms. This is because the EKF is able to fuse the machine vision estimates with the vehicle dynamics model estimates, which fully utilizes the advantages of the two methods and makes the estimation results of the VB-EKF model more accurate.

In addition, machine vision can provide aggregate information about the road, while the

vehicle dynamics model takes into account the motion state and physical characteristics of the vehicle, so the combination of the two can make up for the shortcomings of a single method. Furthermore, the model in this paper can decouple the superposition of vehicle body inclination and road slope angle by discretizing the vehicle longitudinal kinematics equations, so as to obtain the real value of road lateral slope more accurately.

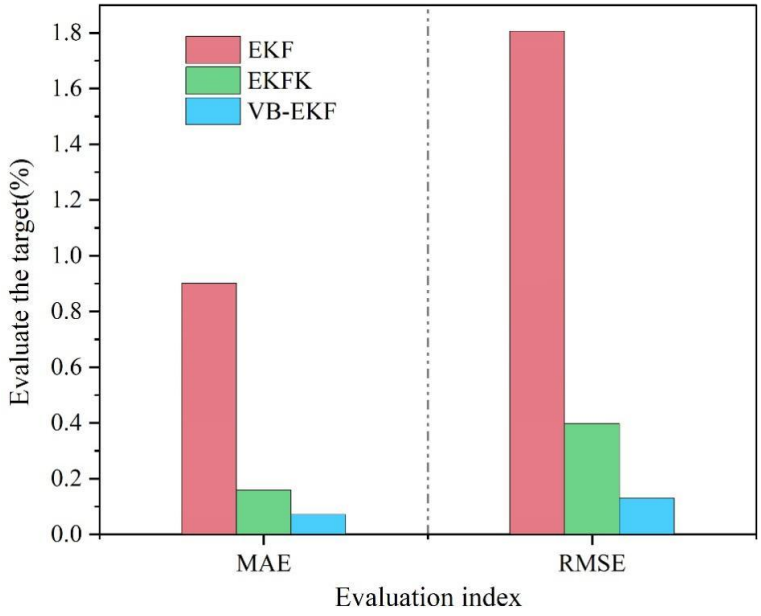

Figure 2: The evaluation of the simulation slope is evaluated objectively

3.1.2 Time dimension estimation results and errors

Figure 3 shows the estimation results and errors in the time dimension, where (a) and (b) represent the results and errors, respectively. It is found that EKF performs very poorly in special conditions, and the large estimation error in special conditions also affects its estimation in the initial stage of non-special conditions.EKFK, because it follows the slope value of the previous moment of the special conditions in special conditions, and the duration of the special conditions is generally shorter except for the stopping condition, in which the road slope does not change, the estimation error of the The estimation error of EKFK is significantly decreased than EKF. However, the estimation error of EKFK is also larger because it stops estimation in special conditions, and usually the braking condition precedes the stopping condition. Therefore, the error in the braking condition will continue to the whole stopping condition, and the estimation result obviously cannot meet the actual demand. On the other hand, VB-EKF can predict the road gradient in special conditions based on the historical gradient data, so the estimation error in special conditions is not much different from that in non-special conditions, and the estimation accuracy of VB-EKF in special conditions is significantly improved compared with that of EKFK.

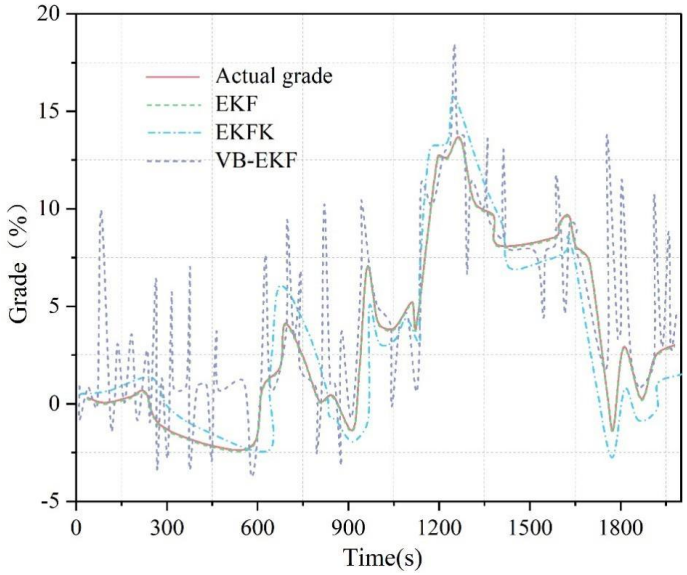

(a)Results

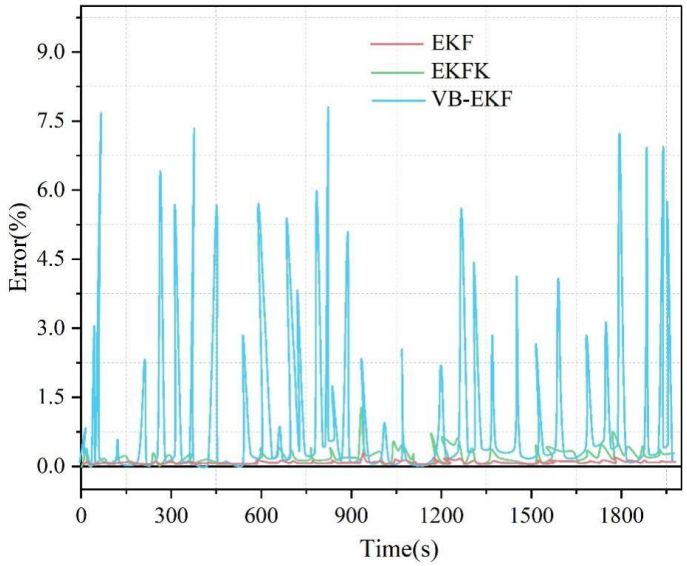

(b)Error

Figure 3: Estimate results and errors of the time dimension

3.1.3 Distance dimension estimation results and errors

Figure 4 shows the estimation results and errors for the distance dimension, where (a) and (b) represent the results and errors, respectively. It can be found that the special working conditions last for mostly shorter mileage, and the situation fits the feature of high accuracy of vision machine (VB) in short sequence prediction, so the application of VB for short-distance gradient prediction in special working conditions makes VB-EKF can follow the trend of gradient change very well with high gradient estimation accuracy, while EKF and EKFK are in stark contrast to it. However, the prediction accuracy of VB becomes worse as the prediction length becomes longer, and if the average speed within the special conditions is higher, the mileage traveled under the special conditions becomes larger and the estimation error of VB becomes

larger. The simulation results validate the effectiveness of the VB-EKF slope estimation method proposed in this paper.

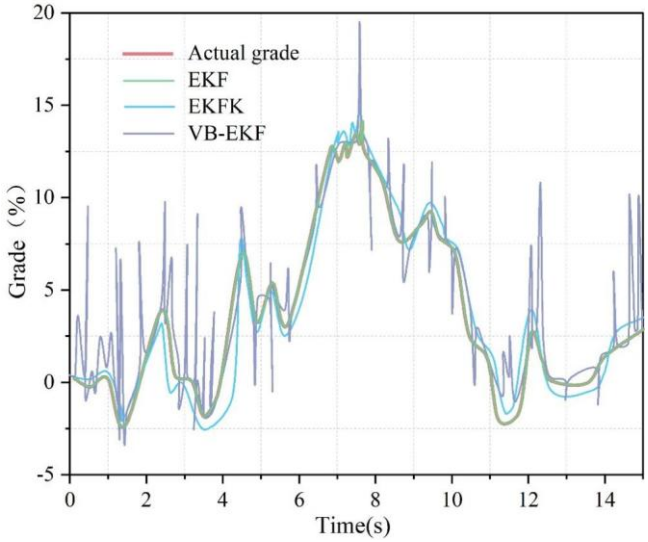

(a)Results

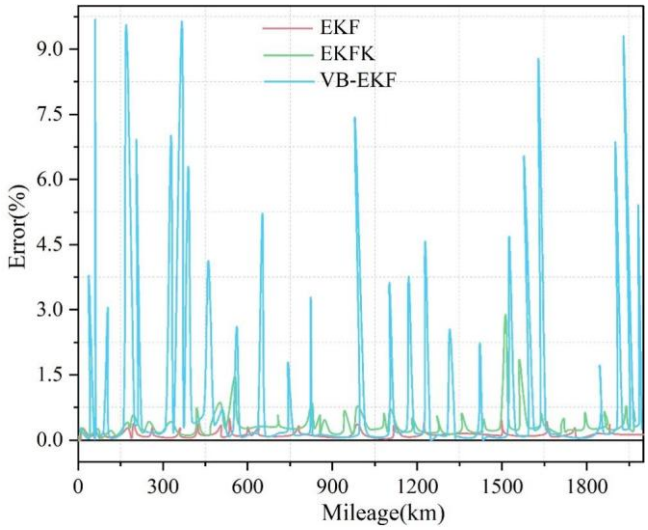

(b)Error

Figure 4: Estimation results and errors of distance dimensions

3.2 Real-vehicle test of VB-EKF-based roadway lateral gradient estimation

The simulation results verify the effectiveness of VB-EKF, and in order to evaluate the effectiveness of the algorithm in real scenarios, real-vehicle road tests are conducted. In this paper, a real vehicle platform of a line-controlled chassis patrol car equipped with a camera and an industrial computer is used to collect the vehicle driving data and the road image in front of the vehicle through the navigation system and the monocular camera, and the communication node is established through the ROS system in the industrial computer to estimate the lateral slope of the road, and the EKF estimation node, VB estimation node and the data fusion node are respectively established, and the results of EKF estimation and VB estimation are fused in

the data fusion node to obtain the final VB-EKF estimation value. The EKF estimation results and VB estimation results are fused in the data fusion node to get the final VB-EKF estimation value, and the test method is the same as above. The trajectory of the test section is a special test interval for vehicle gradient detection in GD province (the whole 15000m), and the gradient value of the test section is measured at fixed points by a level meter, and the elevation is measured every 1m, and the measured roadway elevation is interpolated and fitted to get the real value of the gradient. And under the influence of strong light, the lane lines can still be accurately recognized, and the lateral slope of the road ahead can be estimated by the recognized lane lines.

3.2.1 Analysis of measured results of real-vehicle driving data

The measured results of the real vehicle traveling data are shown in Fig. 5, where (a) and (b) represent the lateral acceleration and transverse swing angular velocity, respectively. The results show that the lateral acceleration and transverse angular velocity of the vehicle in the test process have large oscillations due to the influence of the accuracy of the navigation system.

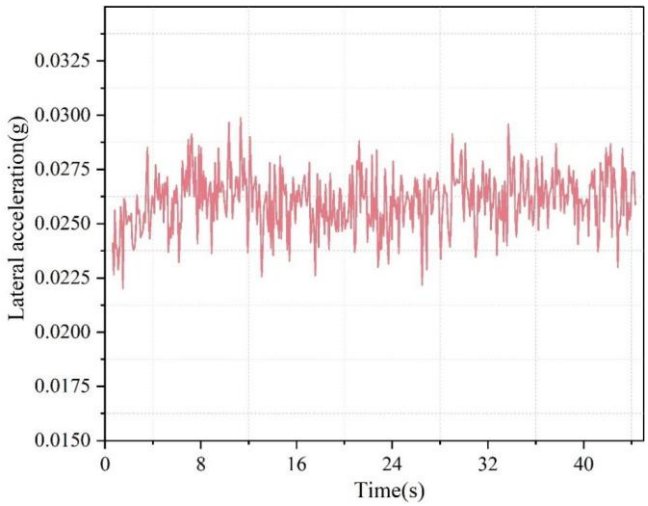

(a)Lateral acceleration

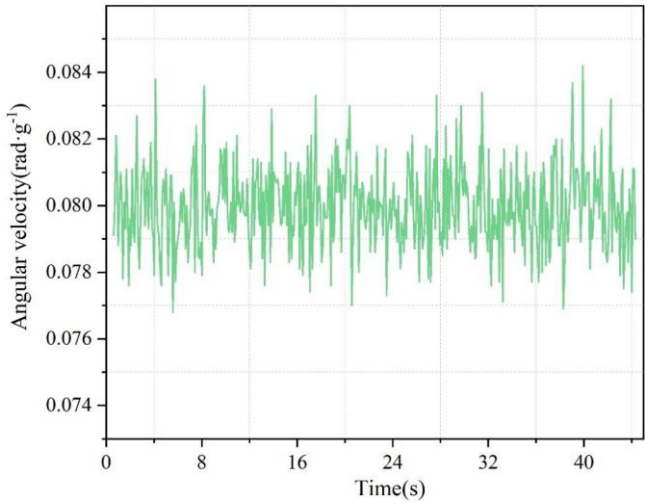

(b)Angular velocity

Figure 5: Real car line driving data measured results

3.2.2 Real vehicle estimation results and errors

The results of the values of the objective evaluation indicators are shown in Figure 6. It can be seen that compared with EKF and EKFK, the VB-EKF model reduces 64.44% and 48.09%, respectively, in the MAE index; and 73.96% and 66.46%, respectively, in the RMSE index. This shows that the real-vehicle estimation results of the model in this paper are associated with lower errors and the model is more generalizable.

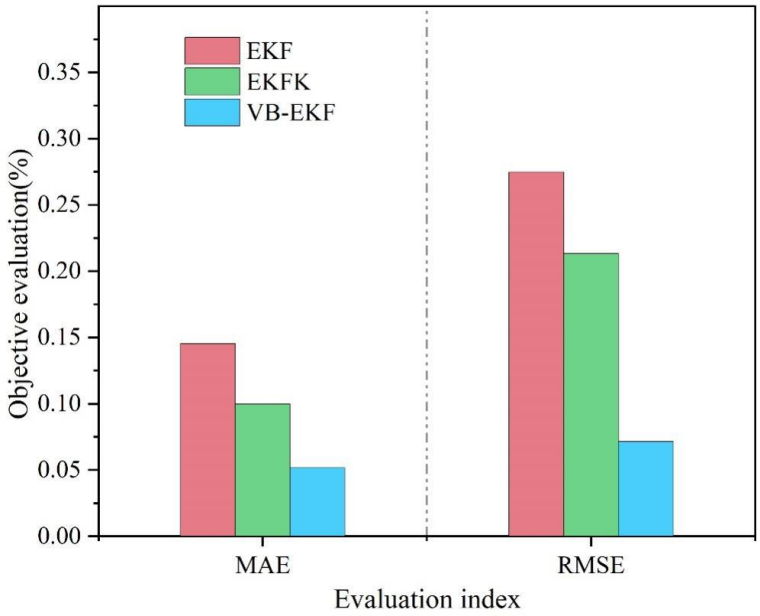

Figure 6: Objective evaluation of the results of the index

In this section, only EKF is used as a comparison model for testing. The estimation results of the real vehicle on the road lateral slope value are shown in Fig. 7, which show that compared with the EKF algorithm, the estimation value of the road lateral slope by the VB-EKF algorithm is closer to the real value.The maximum estimation error of the EKF reaches 6.16%, while the estimation error of the VB-EKF is controlled to be less than 2%, which is a significant decrease compared with the estimation error of the EKF algorithm, and the VB-EKF algorithm has higher stability. From the experimental point of view, the actual vehicle test is more conducive to the improvement of estimation accuracy.

In addition, it may also be due to the measurement accuracy of the inertial navigation system, which leads to the large fluctuation of the data of the lateral acceleration of the vehicle. The relative error of the estimation value of the VB-EKF method is within 2%, which indicates that it can better solve the problem of oscillation of dynamics estimation. Since it takes some time for the algorithm to converge, we speculate that the estimation results will be more accurate with the extension of time.

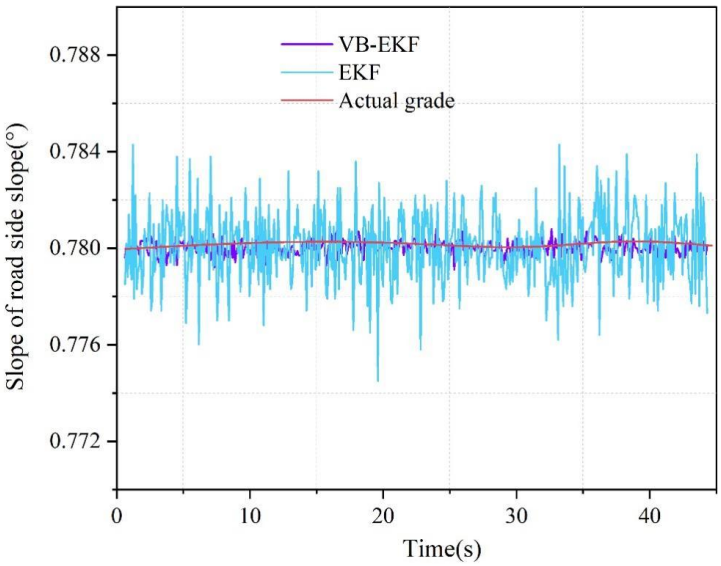

Figure 7: The estimate of the slope of the road side slope

The estimation error of the real vehicle on the value of the lateral slope of the road is shown in Figure 8, the VB-EKF method is more accurate and has a better degree of convergence compared to the EKF algorithm, but the estimation results of the two algorithms in some positions still have a certain degree of error, such as in this paper in the test was found in the two models have a large error between 6~10s. Through analysis, it is concluded that the error may be due to the actual route in the vehicle driving process there is a certain deviation caused.

In addition, this test vehicle is a low-speed electric vehicle, its suspension, tires and other structures and the actual road vehicles have certain differences, especially at higher speeds there may be dynamics of the estimated oscillation of the problem. However, the actual vehicle is smoother and more stable than the low-speed electric vehicle when traveling. From the experimental point of view, the actual vehicle test is more conducive to the improvement of estimation accuracy. Therefore, the road test in this paper does not affect the validity of the algorithm validation even though low-speed electric vehicles are used and tested at low speeds.

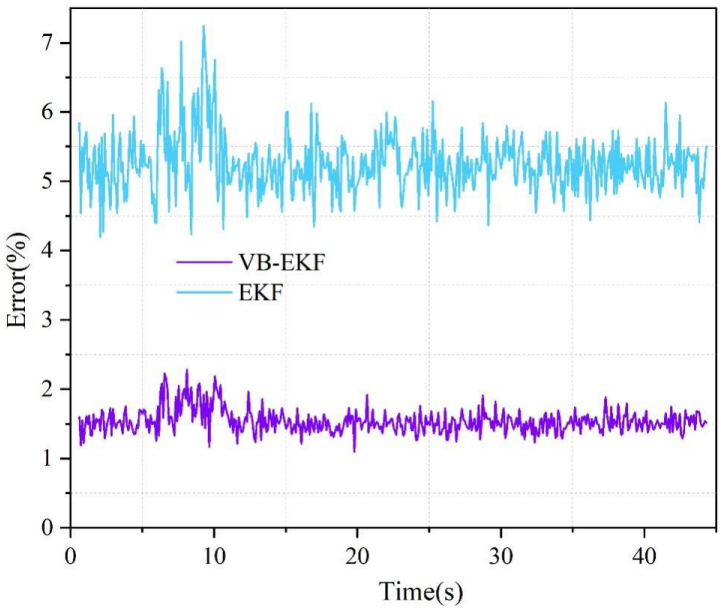

Figure 8: The estimation error of the road side slope value of the real car

4 Conclusion

In order to solve the problem that the existing algorithms are difficult to accurately estimate the lateral slope of the road in the process of dynamic slope detection and automatic tracking and positioning, a road lateral slope estimation method based on the fusion of extended Kalman filter (EKF) and machine vision (VB) is proposed. The simulation and real-vehicle test results show that the VB-EKF algorithm proposed in this paper can estimate the lateral slope of the road ahead more accurately, compared with the EKF algorithm, which significantly improves the slope estimation accuracy, and the average absolute error and the root mean square error in the simulation test have been reduced by 92.13% and 92.85%, respectively, and the oscillation error of the estimation results when the vehicle enters and exits the ramp has been reduced. In the case simulation test, the average absolute error of this paper's model is reduced by 64.44% and 73.96% respectively compared with the comparison model; the RMSE index is reduced by 73.96% and 66.46% respectively; the estimation error can be controlled within 2%, and the model's practical test results are good.

However, although the VB-EKF algorithm greatly improves the estimation accuracy of lateral gradient, the EKF algorithm is based on the 2-degree-of-freedom steady-state model, which will lead to a reduction in the estimation accuracy when the vehicle is traveling at high speed and variable speed, which can be considered in the subsequent high-speed and variable-speed conditions and combined with the change of longitudinal gradient for research.

Funding

This work was supported by the Jiangsu Engineering Research Center for Functional Materials Application and Development.

About the Author

Hui Feng was born in Huai'an, Jiangsu, P.R. China, in 1983. He obtained a doctor's degree from Hohai University in China. He is an Associate Professor with the School of Intelligent Engineering Technology, Jiangsu Vocational and Technical College of Finance and Economics. His research interests include digital image processing, machine learning, and computer vision. He is a member of Jiangsu Association of Artificial Intelligence.huifeng@jscj.edu.cn

Tiewen Lu was born in Xuzhou, Jiangsu, P.R.China, in 1996. She obtained Master's degree from Nanjing Normal University in China. She serves as a teaching assistant at the School of Intelligent Engineering Technology, Jiangsu Vocational and Technical College of Finance and Economics. Her research interests include acoustic signal processing and machine learning. tiewen_lu@163.com

Weiwei Jiang was born in Yangzhou, Jiangsu, P.R. China, in 1995. She obtained a master's degree from China Jiliang University in China. She is an Assistant Teacher with the School of Intelligent Engineering Technology, Jiangsu Vocational and Technical College of Finance and Economics. Her research interests include underwater robot motion control and machine learning. JiangWW9581@yeah.net

Hang Gu was born in Shuyang, Jiangsu, P.R. China. He obtained his Master's degree in Data Science from University of Malaya, Malaysia. He is a Teacher with the School of Intelligent Engineering Technology, Jiangsu Vocational and Technical College of Finance and Economics. His research interests include big data analysis and multimodal sentiment analysis. guhang2011@126.com

References

[1] Salihu, F., Demir, Y. K., & Demir, H. G. (2023). Effect of road slope on driving cycle parameters of urban roads. Transportation research part D: transport and environment, 118, 103676.

[2] Wen, H., Ma, Z., Chen, Z., & Luo, C. (2023). Analyzing the impact of curve and slope on multi-vehicle truck crash severity on mountainous freeways. Accident Analysis & Prevention, 181, 106951.

[3] Duan, J., Peng, Q., & Huang, P. (2022). Slope characteristics of urban construction land and its correlation with ground slope in China. Open Geosciences, 14(1), 1524-1537.

[4] Liu, K., Yamamoto, T., & Morikawa, T. (2017). Impact of road gradient on energy consumption of electric vehicles. Transportation Research Part D: Transport and Environment, 54, 74-81.

[5] Mu, J., Wang, C., Yu, Z., Zhu, X., Yi, G., & Xu, J. (2025). Optimizing freeway maximum gradient and slope length using specific power analysis of five-and six-axle articulated vehicles. Digital Transportation and Safety, 4(1), 50-58.

[6] Yang, Z., Wei, J., Deng, J., & Zhao, S. (2022). An improved method for the evaluation and local multi-scale optimization of the automatic extraction of slope units in complex terrains. Remote Sensing, 14(14), 3444.

[7] Wang, L., Cong, J., Ren, N., Ying, J., Wang, X., Liao, Y., & Liao, Q. (2024). Influence of surface slope on the seeding performance of air-assisted centralized metering device for rapeseed based on numerical simulation. Computers and electronics in agriculture, 218, 108734.

[8] Wang, L., Li, Y., Wu, J., An, Z., Suo, L., Ding, J., ... & Jin, L. (2023). Effects of the rainfall intensity and slope gradient on soil erosion and nitrogen loss on the sloping fields of miyun reservoir. Plants, 12(3), 423.

[9] Seyedashraf, O., Bottacin-Busolin, A., & Harou, J. J. (2021). Many-objective optimization of sustainable drainage systems in urban areas with different surface slopes. Water Resources Management, 35(8), 2449-2464.

[10] Shih, H. H., Chien, C. Y., Huang, H. S., Lai, Z. F., Yeh, P. Y., & Chuang, C. T. (2024, October). Road Slope Estimation Using Field-Adjustable Stereo Vision. In 2024 International Automatic Control Conference (CACS) (pp. 1-6). IEEE.

[11] Ustunel, E., & Masazade, E. (2019). Vision-based road slope estimation methods using road lines or local features from instant images. IET Intelligent Transport Systems, 13(10), 1590-1602.

[12] Yan, Y., & Li, H. (2022). Machine vision-based method for estimating lateral slope of structured roads. Sensors, 22(5), 1867.

[13] Rúa, E., Núñez-Seoane, A., Arias, P., & Martínez-Sánchez, J. (2023). Automatic detection to inventory road slopes using open LiDAR point clouds. International Journal

of Applied Earth Observation and Geoinformation, 118, 103225.

[14] Thammaboribal, P., Tripathi, N. K., Nakamura, S., & Lipiloet, S. (2025). Determinations of the Slope of the Chao Phraya Riverbank and Manning's Roughness Coefficient Utilizing Precise Point Positioning (PPP) Measurement Technique. International Journal of Geoinformatics, 21(2).

[15] Yeh, C. H., Lin, M. L., Chan, Y. C., Chang, K. J., & Hsieh, Y. C. (2017). Dip-slope mapping of sedimentary terrain using polygon auto-tracing and airborne LiDAR topographic data. Engineering Geology, 222, 236-249.

[16] Khodarahmi, M., & Maihami, V. (2023). A review on Kalman filter models. Archives of Computational Methods in Engineering, 30(1), 727-747.

[17] Yang, J., Ma, J., Liu, X., Qi, L., Wang, Z., Zhuang, Y., & Shi, L. (2017). A height constrained adaptive Kalman filtering based on climbing motion model for GNSS positioning. IEEE Sensors Journal, 17(21), 7105-7113.

[18] Zhao, M., Yang, F., Sun, D., Han, W., Xie, F., & Chen, T. (2018, June). A joint dynamic estimation algorithm of vehicle mass and road slope considering braking and turning. In 2018 Chinese Control And Decision Conference (CCDC) (pp. 5868-5873). IEEE.

[19] Guo, J., He, C., Li, J., & Wei, H. (2022). Slope estimation method of electric vehicles based on improved Sage–Husa adaptive Kalman filter. Energies, 15(11), 4126.

[20] Akop Antonyan,Aleksandr Klimov,Andrey Buchkin,Andrey Keller,Sergey Shadrin,Daria Makarova & Yury Furletov. (2025). Developing an Algorithm Limiting the Longitudinal Acceleration of an Electric Vehicle. Vehicles,7(1),7-7.

[21] Tim J van der Zee,Paolo Tecchio,Daniel Hahn & Brent J Raiteri. (2025). UltraTimTrack: a Kalman-filter-based algorithm to track muscle fascicles in ultrasound image sequences.. PeerJ. Computer science,11,e2636.

[22] Meng Xue & Baolong Liu. (2024). An Adaptive Strong Tracking Volume Kalman Filter Algorithm. Journal of Physics: Conference Series,2872(1),012045-012045.

[23] Lai Xin,Li Yueyang & Zhang Qican. (2024). Background-extracted extended Kalman filter-based phase shift estimation algorithm for phase shifting profilometry system. Optics and Laser Technology,170,

[24] Yunfeng Ge,Shiyu Yuan,Kaili Chen & Huiming Tang. (2024). Estimation of rock joint roughness using binocular stereo vision. Measurement,234,114881-.